



Repositorio Institucional de la Universidad Autónoma de Madrid

<https://repositorio.uam.es>

Esta es la **versión de autor** del artículo publicado en:
This is an **author produced version** of a paper published in:

British Journal of Pharmacology (2020): 10 March

DOI: <https://doi.org/10.1111/bph.15048>

Copyright: © 2020 The British Pharmacological Society

El acceso a la versión del editor puede requerir la suscripción del recurso

Access to the published version may require subscription

Ruiz-Hurtado Gema (Orcid ID: 0000-0003-3482-0915)

Delgado Carmen (Orcid ID: 0000-0002-0047-4674)

BENEFICIAL EFFECTS OF PARICALCITOL ON CARDIAC DYSFUNCTION AND REMODELLING IN A MODEL OF ESTABLISHED HEART FAILURE

Running Head: Paricalcitol in established heart failure

MARÍA TAMAYO¹, LAURA MARTÍN-NUNES¹, ALMUDENA VAL-BLASCO², MARIA JOSÉ G.M-PIEDRAS³, JOSÉ ALBERTO NAVARRO-GARCÍA⁴, EDUARDO LAGE⁵, PATRICIA PRIETO¹, GEMA RUIZ-HURTADO⁴, MARÍA FERNÁNDEZ-VELASCO^{2*}, CARMEN DELGADO^{1*}.

¹Biomedical Research Institute “Alberto Sols” CSIC-UAM/CIBER-CV, Madrid, Spain.

²Innate Immune Response Group, IdiPAZ/CIBER-CV, La Paz University Hospital, Madrid, Spain.

³Universidad Francisco de Vitoria, Madrid, Spain.

⁴Cardiorenal Translational Laboratory, Institute of Research i+12, CIBER-CV, Hospital Universitario 12 de Octubre, Madrid, Spain

⁵Department of Electronics and Communications Technology, Universidad Autónoma de Madrid, Madrid, Spain

* Corresponding authors:

Carmen Delgado, Ph.D.

Instituto de Investigaciones Biomédicas “Alberto Sols”

Arturo Duperier 4

28029 Madrid, Spain

Phone: +34 915854432

Email: cdelgado@iib.uam.es

This article has been accepted for publication and undergone full peer review but has not been through the copyediting, typesetting, pagination and proofreading process which may lead to differences between this version and the Version of Record. Please cite this article as doi: 10.1111/bph.15048

Or

María Fernández-Velasco, Ph.D

Instituto de Investigación Hospital la Paz, Idipaz

Paseo de la Castellana 261

28046 Madrid. Spain

Phone: +34 914972747

Email: maria.fernandez@idipaz.es

Competing Interests's Statement: none

Abstract

Background and Purpose

The synthetic vitamin D₃ analog paricalcitol acts as a selective activator of vitamin D receptor (VDR). While there is evidence for cardioprotective effects of paricalcitol associated with the VDR pathway, less information is available about the structural and functional cardiac effects of paricalcitol on established heart failure (HF), and particularly its effects on associated electrophysiological or Ca²⁺-handling remodelling.

Experimental Approach

We used a murine model of transverse aortic constriction (TAC) to study the effect of paricalcitol on established HF. Treatment was initiated 4 weeks after surgery over 5 consecutive weeks and mice were sacrificed 9 weeks after surgery. Cardiac magnetic resonance imaging (CMRI) was performed 4 and 9 weeks after surgery. Hearts were used for biochemical and histological studies and to isolate ventricular myocytes for electrophysiological and calcium imaging studies.

Key Results

CMRI analysis revealed that, compared with vehicle, paricalcitol treatment prevented the progression of ventricular dilation and hypertrophy after TAC and halted the corresponding decline in ejection fraction. These beneficial effects were related to the attenuation of intracellular Ca²⁺-mishandling remodelling, antifibrotic and antihypertrophic effects, and potentially antiarrhythmic effects by preventing the reduction of K⁺ current density and the long QT, JT and TpTe intervals observed in HF animals.

Conclusions and implications

The results suggest that paricalcitol treatment in established HF hampers disease progression and improves adverse electrophysiological and Ca²⁺ handling remodelling, attenuating the vulnerability to HF-associated ventricular arrhythmias. Paricalcitol may emerge as a potential therapeutic option in the treatment of HF.

Key words: Paricalcitol, K⁺ currents, transverse aortic constriction, heart failure, electrophysiological remodelling, Ca²⁺ handling remodelling, cardiac fibrosis, QT interval, JT interval, TpTe interval.

Abbreviations

Parathyroid hormone (PTH), heart failure (HF), left ventricle (LV), ejection fraction (EF), cardiac magnetic resonance imaging (CMRI), vitamin D receptor (VDR), transverse aortic constriction (TAC), left ventricular mass (LVM), left ventricular hypertrophy (LVH), left ventricle end-diastolic volume (LVEDV), left ventricle end-systolic volume (LVESV), left ventricular ejection fraction (LVEF) heart weight (HW), tibia length (TL), sarcoplasmic reticulum (SR), heart rate (HR). Ventricular electrocardiographic repolarization parameters: interval between QRS end J point and the end of the T wave (JT interval), the interval from the peak to the end of the T wave (TpTe), the fast transient outward current (I_{tof}), the ultrarapid delayed rectifier K^+ current (I_{kur}) and the non-inactivating steady-state outward current (I_{ss}).

BULLET POINT SUMMARY

What is already known:

- ✓ Depressed cardiac function in HF is commonly associated with impairment of Ca_i^{2+} handling.
- ✓ HF is associated with an increased incidence of malignant arrhythmias and sudden death.

What this study adds:

- ✓ Paricalcitol treatment on established HF prevents Ca^{2+} mishandling
- ✓ Paricalcitol treatment counteracts the down-regulation of K^+ currents associated with HF.

Clinical significance:

- ✓ Paricalcitol treatment reduces LVH, fibrosis and adverse electrophysiological and Ca^{2+} handling remodelling.
- ✓ Paricalcitol might emerge as a potential therapeutic option in the treatment of HF.

INTRODUCTION

Chronic heart failure (HF) is a major public health concern in ageing societies and a leading cause of hospitalisation and mortality (Ponikowski et al., 2014, Savarese and Lund, 2017). The disorder is usually accompanied by progression from adaptive to maladaptive hypertrophy and also cardiac dilation and diminished left ventricular ejection fraction (LVEF). Adverse cardiac remodelling is an important determinant of the clinical outcome of HF and is linked to disease progression and poor prognosis (Heusch et al., 2014). Ventricular remodelling encompasses cardiomyocyte hypertrophy, pro-fibrotic responses and downregulation of K^+ currents, which alter the electrotonic coupling between cells and prolongs QT intervals, overall increasing the risk of ventricular arrhythmias and sudden cardiac death (Nass et al., 2008, Tomaselli et al., 1994). Depressed cardiac function in HF is also commonly associated with impairment of intracellular Ca^{2+} handling. In this regard, failing hearts often show depressed systolic Ca^{2+} release and lower sarcoplasmic reticulum (SR)- Ca^{2+} load, which compromises cell contractility (Val-Blasco et al., 2017, Gómez-Hurtado et al., 2017, Ruiz-Hurtado et al., 2015).

Over the past 25 years, considerable progress has been made in the treatment of chronic HF using angiotensin-converting enzyme inhibitors and angiotensin II type 1 receptor blockers, and also mineralocorticoid receptor antagonists, β -receptor blockers and resynchronisation therapy (Owens et al., 2016). The pharmacological treatment of HF aims to halt progressive cardiac hypertrophy and LVEF decline; however, as many as 25–40% of all patients die from chronic HF within 1 year of diagnosis. New therapies are entering clinical trials yearly (Nabeebaccus et al., 2016, Tamargo et al., 2018), but the identification of new targets with therapeutic potential in HF continues to be an area of great interest.

Paricalcitol (19-nor-1 α , 25-dihydroxyvitamin D₂) is a synthetic vitamin D₃ analog that acts as a selective activator of the vitamin D receptor (VDR), and is indicated for the prevention and treatment of secondary hyperparathyroidism associated with chronic kidney disease (Robinson and Scott, 2005). There is a growing body of work demonstrating beneficial cardioprotective properties associated with the VDR pathway (Gardner et al., 2013, Meredith and McManus, 2013, Norman and Powell, 2014). Yet, little information is available on the cardiac structural and functional effects of paricalcitol on established HF. Likewise, there is a paucity of evidence on the effect of paricalcitol on arrhythmogenic disorders, or Ca^{2+} handling remodelling associated with established HF.

In the present study, we used a murine model of HF induced by pressure overload (transverse aortic constriction, TAC) to test the hypothesis that paricalcitol treatment blocks the progression of the disease and has cardioprotective effects on adverse Ca^{2+} handling and electrical remodelling.

METHODS

Animals

Male C57BL/6J mice (24-29 g, 10 weeks of age) were used in all experiments. Mice were bred and housed under specific pathogen-free conditions in the Experimental Animal Centre of the Biomedical Research Institute “Alberto Sols” CSIC-UAM/CIBER-CV, Madrid, Spain. All experiments were performed after approval of the Bioethical Committee of the *Consejo Superior de Investigaciones Científicas* (Proex 035-15), following the guidelines for ethical care of experimental animals of the European Union (2012/63/EU) and in accordance with the ARRIVE guidelines for reporting experiments involving animals (Kilkenny et al., 2010, McGrath et al., 2010). Animals were maintained at controlled temperature (23–25°C) on a 12-hour light/dark cycle with *ad libitum* access to water and a standard diet (Teklad Global 14% Protein Rodent maintenance Diet, Harlan Laboratories Inc., Indianapolis, IN) that contained 600 IU g⁻¹ of vitamin D₃ (cholecalciferol). The animal cages (Polysulfone type SII, Techniplast, Italy) were 553 cm² by 20.8 cm depth and animals were housed with a maximum of 4 mice per cage.

Transverse aortic constriction

Animals were anaesthetised by i.p. injection of a mixture of ketamine (100 mg kg⁻¹) and xylazine (10 mg kg⁻¹). Adequacy of anesthesia was determined by assessing loss of withdrawal reflex. Mice were then intubated and underwent trans-sternal thoracotomy. The transverse aorta was constricted with a 6-0 black braided silk suture tied against a 27-gauge needle, as described by Rockman (Rockman et al., 1991). A similar procedure was followed for sham-operated mice, but no suture was tied. Mice were given subcutaneous buprenorphine (1 mg kg⁻¹) for pain relief before and after the surgery. A heated pad was used during surgery to minimise discomfort and maintain body temperature.

Study design

A scheme of the experimental approach is shown in Figure 1. Animals were distributed into two experimental groups: SHAM-operated and TAC-operated. Cardiac structure and function were analysed by cardiac magnetic resonance imaging (CMRI) 4 weeks after surgery. At this point, only TAC operated mice with EF <58% and with significant LV dilation were included in the TAC group. The mice were then blind randomised to the vehicle or paricalcitol treatment groups, with each group originally consisting of 16 mice. Treatment with vehicle (water for injection, 3.9% propylene glycol and 1.3% ethyl alcohol) or with, 300 ng kg⁻¹ paricalcitol (Normon S.A. Madrid, Spain) was delivered by i.p. injection 3 times weekly (Monday, Wednesday and Friday) for 5 consecutive weeks. CMRI was repeated after the 5 weeks of treatment (9 weeks after the surgery). Also, a standard ECG was performed and blood samples were drawn from the retro-orbital plexus. Finally, mice were sacrificed and hearts were excised, weighed and prepared for biochemical and histological studies. In some experiments, hearts were retrogradely perfused through the aorta using a modified Langendorff apparatus to isolate ventricular myocytes (see below).

CMRI data pre-surgery were not performed because the aim of the study was to analyze the effect of paricalcitol on established HF. Therefore, control values were those obtained in the SHAM group 4 and 9 weeks after the surgery.

Macroscopic parameters, cell capacitance and serum analysis

The heart weight (HW) to tibia length (TL) ratio was measured as an index of cardiac hypertrophy (Table 1). Cardiomyocyte surface area was quantified using LSM Zeiss Image Browser 4.2 software (Carl Zeiss, Germany) (Table 1) and the membrane capacitance of the cardiomyocytes was evaluated using the whole-cell configuration of the patch-clamp technique (see below) (Table 1). Blood samples were centrifuged at 2500 rpm for 5 min to obtain blood serum. A parathyroid hormone (PTH) assay was performed using the Mouse PTH 1-84 ELISA Kit (Immutopics, San Clemente, CA). Calcium and phosphorus assays were performed using colorimetric assays kits (Calcium Assay Kit and Phosphate Assay Kit, respectively; Abcam, Cambridge, UK) on an EnSpireTM Multimode Plate Reader (Perkin Elmer, Waltham, MA).

Cardiac magnetic resonance imaging

CMRI was carried out on a 7.0 Tesla MR system (Bruker Pharmascan, Bruker, Ettlingen, Germany). Analysis was performed in the Biomedical Research Institute “Alberto Sols” CSIC-UAM. Mice were anaesthetised with an isoflurane and oxygen mixture (2% in 1L min⁻¹ for induction and 1.5% during the acquisition). The temperature of the animals was monitored and maintained at 35–36°C during the experiments. Heart and respiratory rates were recorded using the 1025 SAM monitoring and gating system (SA Instruments, Inc., New York, NY). Several images were acquired to localise the short axis planes. After position adjustment, 6 to 12 slices were acquired to cover the entire heart. Each slice consisted of 20 gated frames synchronised with the cardiac cycle. For image acquisition, we used the Intradate FLASH sequence with the following parameters: echo time (TE) = 1.262 ms; field of view (FOV) = 3 × 3 cm²; slice thickness = 0.8 mm; matrix size = 256 × 256. The acquired data were zero-filled to achieve a reconstructed matrix size of 256 × 256. Images were analysed using SEGMENT v2.0 R5642 (<http://segment.heiberg.se>). Six slices were selected from each heart and analysed by manual segmentation of left ventricular endocardial and epicardial borders in all the image frames. After segmentation of the images, SEGMENT was used to automatically calculate the following functional parameters: left ventricle end-diastolic volume (LVEDV) (μL) and left ventricle end-systolic volume (LVESV) (μL), ejection fraction (EF) (%) and left ventricle mass (LVM) (mg). LVM was estimated by LV wall volume × the specific gravity of the myocardium (1.05 g/cm³).

ECG recordings

ECG recordings were obtained on the Small Animal Physiological Monitoring System (Harvard Apparatus, Holliston, MA). Mice were located in prone position on a warm pad at 37°C during the recordings and were lightly anaesthetised with an isoflurane and oxygen mixture (1.5%). ECG recordings were obtained under basal conditions for 5 minutes. ECG registries were converted into LabChart binary files using a cross-platform Java program. Files were analysed in a blinded fashion using LabChart 7.0 software (AD Instruments, Sydney, Australia) (RRID:SCR_017551).

Histology

Sirius red staining was performed on paraffin sections to measure fibrosis. Tissue samples were dehydrated, embedded in paraffin and cut into sections (5-μm thickness). Slices were

stained with sirius red (Direct Red 80) (25 mL of 10% aqueous Direct Red in 225 mL of 1.3% aqueous picric acid; Sigma-Aldrich Chemical Company, Madrid, Spain). Quantification of collagen content was performed using ImageJ software (NIH) (RRID:SCR_003070) and expressed as the perivascular fibrosis area divided by vessel lumen area, and as a percentage of interstitial fibrosis over the total amount of tissue, excluding lumen and perivascular fibrosis. A single investigator blinded to the experimental groups performed the analysis.

Total RNA isolation and real-time PCR

Total RNA was extracted from a portion of the left ventricle of representative mice of each experimental group using the RNeasy Mini Kit on a QIAcube robotic workstation (both from Qiagen, Hilden, Germany) and was quantified using a NanoDrop spectrophotometer (NanoDrop Technologies, Wilmington, DE). In total, 250 ng of RNA was retrotranscribed using the High-Capacity cDNA Reverse Transcription Kit (Applied Biosystems, Foster City, CA) and real-time PCR was performed on an ABI 7900HT Fast Real-Time PCR platform (Applied Biosystems). The endogenous *Rplp0* gene (36B4) was used as reference for fold-induction calculations using the $\Delta\Delta C_t$ method.

The following primers were purchased from Invitrogen (Carlsbad, CA):

m-Nppa-F: ATTGACAGGATTGGAGCCCAGAGT
m-Nppa-R: TGACACACCACAAGGGCTTAGGAT

m-Rcan1.4: F: GAGCGAGTCGTTTCGTTAAGC
m-Rcan1.4-R: GCCACACAAGCAATCAGGGA

m-Serpine1-F: CGGCAGATCCAAGATGCTATG
m-Serpine1-R: GACCAGCTCTAGGTCCCGCT

m-Coll1a1-F: AATGGCACGGCTGTCTGCGA
m-Coll1a1-R: AGCACTCGCCCTCCCGTCTT

m-Col3a1-F: CTGTAACATGGAAACTGGGGAAA
m-Col3a1-R: CCATAGCTGAACTGAAAACCACC

m-Atp2a2-F: TAAATGCCCCGCTGTTTTGCT
m-Atp2a2-R: TTGTCATCTGCCAGGACCAT

m-Pln-F: ACCGAAGCCAAGGTCTCCTA
m-Pln-R: TCCATTATGCCAGGAAGGCAA

m-Rplp0-F: AGATGCAGCAGATCCGCAT
m-Rplp0-R: GTTCTTGCCCATCAGCACC

Cardiomyocyte isolation

Adult single ventricular cardiomyocytes were isolated as reported previously (Delgado et al., 2015). Briefly, mice were heparinised and anaesthetised with ketamine (100 mg kg⁻¹) and xylazine (10 mg kg⁻¹) by i.p. injection. Adequacy of anesthesia was determined by assessing loss of withdrawal reflex. Hearts were then rapidly removed and retrogradely perfused through the aorta using a modified Langendorff apparatus. Hearts were perfused for 2–3 min at 36–37°C with a standard calcium-free Tyrode's solution containing 0.2 mM EGTA, and then for 3–4 min with the same Tyrode's solution containing collagenase type II (251 IU mL⁻¹, Worthington Biochemical, Lakewood, NJ) and 0.1 mM CaCl₂. After perfusion, the hearts were removed from the Langendorff apparatus and the ventricles were chopped into small pieces and gently stirred for 2–5 min in a standard Tyrode's solution containing 0.1 mmol L⁻¹ CaCl₂, collagenase (251 IU mL⁻¹) and BSA (Sigma-Aldrich) to disperse the isolated ventricular myocytes. Cell suspensions were filtered through a 250 µm nylon mesh, pelleted by centrifugation for 3 min at 20 × g and suspended in Tyrode's solution containing 0.5 mmol L⁻¹ CaCl₂ and BSA. Cells were centrifuged as before and suspended in a storage solution containing 1 mmol L⁻¹ CaCl₂ and BSA. Standard calcium-free Tyrode's solution contained in mmol L⁻¹: 130 NaCl, 5.4 KCl, 0.4 NaH₂PO₄, 0.5 MgCl₂, 25 HEPES, 22 glucose; the pH was adjusted to 7.4 with NaOH. Single rod-shaped and Ca²⁺-tolerant cells with clear cross-striations were used for electrophysiological and intracellular Ca²⁺ imaging studies.

Electrophysiological studies

Isolated ventricular myocytes were placed in a chamber mounted on the stage of an inverted microscope and allowed to adhere for 5 min before being superfused with external solution. Whole-cell voltage-clamp recordings were obtained in the ruptured patch configuration using an Axopatch 200B patch clamp amplifier (Molecular Devices, Sunnyvale, CA). The patch pipette resistance for K⁺ current recordings was 1–2 MΩ and was filled with a solution containing in mmol L⁻¹: 135 KCl, 4 MgCl₂, 5 EGTA, 10 HEPES, 10 glucose, 5 Na₂ATP, and 3 disodium creatine phosphate; the pH was adjusted to 7.2 with KOH. Whole-cell voltage clamp experiments were performed at room temperature (24–26°C).

In the adult mouse ventricle, the repolarising K⁺ currents involve three components that can be identified by their specific voltage dependence and their sensitivity to pharmacological

agents. First, total K^+ currents (I_{K^+}) were elicited by applying 300 ms depolarising steps from -50 mV to +50 mV (with 10 mV steps) from a holding potential of -80 mV at a frequency of 0.2 Hz. Then, the fast transient outward current (I_{tof}), the ultrarapid delayed rectifier K^+ current (I_{kur}) and the non-inactivating steady-state outward current (I_{ss}) were obtained as previously reported (Tamayo et al., 2018). The external solution for I_{K^+} recordings contained in mmol L^{-1} : 135 NaCl, 10 glucose, 10 HEPES, 1 $MgCl_2$, 1 $CaCl_2$, 4 KCl, and 2 $CoCl_2$; the pH was adjusted to 7.4 with NaOH.

L-type Ca^{2+} currents (I_{CaL}) were elicited by applying 300 ms depolarising voltage pulses from a holding potential of -50 mV, between -40 to +60 mV (with 10 mV steps) at a frequency of 0.2 Hz. Ca^{2+} currents were normalised to cell capacitance to obtain current density. The external Tyrode's solution for I_{CaL} recordings contained in mmol L^{-1} : 140 NaCl, 1.1 $MgCl_2$, 5.4 CsCl, 10 glucose, 5 HEPES, 1.8 $CaCl_2$; the pH was adjusted to 7.4 with CsOH. The intracellular recording pipette solution for whole-cell experiments contained in mmol L^{-1} : 100 CsCl, 20 TEACl, 5 EGTA, 10 HEPES, 5 Na_2ATP , 0.4 Na_2GTP , 5 Na_2 creatine phosphate, 0.06 $CaCl_2$; the pH was adjusted to 7.2 with CsOH.

Current density was calculated from peak K^+ currents or current amplitude (I_{CaL}) normalised to the membrane capacitance. Membrane capacitance (C_m) (Table 1) was elicited by applying ± 10 mV voltage steps from -60 mV and C_m was calculated according to the following equation:

$$C_m = \tau_c I_0 / V_m [1 - (I_\infty / I_0)]$$

where τ_c is the time constant of the membrane capacitance, I_0 the maximum capacitance current value, V_m the amplitude of the voltage step, and I_∞ the amplitude of the steady-state current.

Intracellular Ca^{2+} dynamics

Changes in intracellular Ca^{2+} concentration ($[Ca^{2+}]_i$) were recorded in intact isolated cardiomyocytes. Cardiomyocytes were loaded with the fluorescent Ca^{2+} dye Fluo-3 acetomethyl ester (Fluo-3 AM, Invitrogen) (5 $\mu mol L^{-1}$). All recordings were carried out at room temperature (20–23°C). Images were recorded on a Meta Zeiss LSM 710 confocal microscope (40 \times oil inversion objective with a 1.2 NA), by scanning cells with an Argon laser every 1.54 s. Fluo-3 AM was excited at 488 nm and the emitted fluorescence was

collected at >505 nm. $[Ca^{2+}]_i$ transients were recording in Fluo-3AM-loaded cardiomyocytes electrically stimulated at 2 Hz. The amplitude of $[Ca^{2+}]_i$ transients (F/F_0) was calculated by normalising the maximal fluorescence by the basal fluorescence. Subtraction of the background fluorescence was carried out beforehand in both cases. Therefore, we calculated F/F_0 as: $(F - \text{background}) / (F_0 - \text{background})$. The decay time constant of Ca^{2+} transients (τ) was measured by fitting the decay trace. Ca^{2+} sparks were recorded in quiescent cells and identified using an automated detection system and by employing a criterion that discriminated the detection of false events, as previously reported (Gómez-Hurtado et al., 2017). SR- Ca^{2+} load was determined by rapid caffeine (10 mmol L⁻¹) administration to deplete the SR of Ca^{2+} stores, after field-stimulation to reach the steady state of Ca^{2+} load.

SERCA2a activity (k SERCA2a) was indirectly determined by subtracting the decay rate constant of caffeine-evoked $[Ca^{2+}]_i$ transients from the decay rate constant of systolic $[Ca^{2+}]_i$ transients (Bode et al., 2011, Delgado et al., 2015).

Data analysis was performed with homemade routines using IDL 8 software (Research System Inc. Boulder, CO) and designed by AM Gómez (UMR-S 1180, INSERM). Images were corrected for background fluorescence. Cardiomyocyte surface area was quantified with LSM Zeiss Image Browser 4.2 software (Carl Zeiss) (Table 1).

Data and statistical analysis

The data and statistical analysis comply with the recommendations on experimental design and analysis in pharmacology (Curtis et al., 2018). Data are expressed as mean \pm SEM or mean \pm SD when individual values were included in the plot. Statistical analysis was performed using GraphPad Prism v.6.0 (GraphPad Software Inc., La Jolla, CA) (RRID:SCR_002798). One-way ANOVA was used to compare significance among groups. If ANOVA produced a significant value of F ($p < 0.05$) and there was no significant variance inhomogeneity, Bonferroni's post hoc multicomparison analysis was applied. Paired Student's t-test was used for comparison of resonance magnetic imaging data obtained in the same mouse 4 weeks and 9 weeks after surgery. All p-values were two-tailed and p-values < 0.05 were considered as statistically significant. Statistical analysis was undertaken only for studies where each group size was at least 5. N = number of mice and n = number of

independent cardiomyocytes. The data that support the findings of this study are available from the corresponding author upon reasonable request.

Nomenclature of Targets and Ligands

Key protein targets and ligands in this article are hyperlinked to corresponding entries in <http://www.guidetopharmacology.org>, the common portal for data from the IUPHAR/BPS Guide to PHARMACOLOGY (Southan et al., 2016), and are permanently archived in the Concise Guide to PHARMACOLOGY 2015/16 (Alexander et al., 2015a, 2015b).

RESULTS

Paricalcitol treatment prevents the progression of established cardiac hypertrophy and heart failure

Cardiac structure and function were evaluated by CMRI in the same mouse 4 weeks and 9 weeks after the surgery. Figure 2A-D shows individual values of LVM, LVEDV, LVESV and EF, 4 weeks after the surgery, just prior to vehicle or paricalcitol treatment. LVM, LVEDV and LVESV were significantly increased and EF decreased in both TAC groups compared with sham groups. Moreover, there were no differences between the TAC and TAC-paricalcitol groups in any parameter before starting the treatment. Figure 3A shows CMR images of representative hearts 9 weeks after surgery; specifically, 4-chamber long-axis (upper panel) and 2-chamber short-axis (lower panel) views from the 4 experimental groups (sham, sham-paricalcitol, TAC and TAC-paricalcitol). The results of this analysis are shown in Figure 3B–E. Evaluation of LVM is represented in Figure 3B, and showed that LVM was maintained in both sham groups from 4 to 9 weeks. As mentioned, LVM was significantly higher in the TAC groups than in the sham groups 4 weeks after surgery. Notably, whereas LVM continued to increase over the next 5 weeks in the TAC-vehicle group, it remained stable in the TAC-paricalcitol group. These data strongly suggest that paricalcitol has a significant effect on preventing increases in cardiac mass in the setting of established cardiac hypertrophy. Quantification of the CMRI parameters LVEDV and LVESV is shown in Figure 3C and 3D, respectively. Both parameters significantly increased 4 weeks after the TAC surgery when compared with the sham group, indicating a dilation of the left ventricle (LV) that was significantly greater 9 weeks after the surgery. Treatment with paricalcitol for 5 weeks once the LV dilation was present, significantly prevented the progression of both parameters. Consistent with these changes, the EF was significantly lower in the TAC groups

than in equivalent sham groups at 4 weeks after surgery (Figure 3E). The EF further decreased in the TAC-vehicle group at 9 weeks after surgery, whereas treatment with paricalcitol during 5 weeks inhibited the decline in EF. Taken together, these data suggest that paricalcitol blocks the functional and structural deleterious remodelling in this model of established HF. In addition, the beneficial effects of paricalcitol occurred in the absence of an increase in the serum concentration of Ca^{2+} or phosphate, but with a significant decrease in PTH indicating that the drug effectively activates VDR (Table 1).

Paricalcitol improves $[\text{Ca}^{2+}]_i$ mishandling remodelling associated with established heart failure

Given that cardiac dysfunction and Ca^{2+} mishandling are closely related, we next determined whether the beneficial effects of the paricalcitol treatment regime were associated with changes to intracellular Ca^{2+} dynamics.

First, we analysed the I_{CaL} in cardiomyocytes using the patch-clamp technique in the whole cell configuration. As shown in Figure 4A, the mean values of current-voltage (IV) density curves for I_{CaL} were similar between the 4 groups. We examined systolic Ca^{2+} release by the analysis of $[\text{Ca}^{2+}]_i$ transients in isolated cardiomyocytes field stimulated at 2 Hz. Figure 4B shows representative line-scan confocal images of $[\text{Ca}^{2+}]_i$ transients in cells from the 4 groups. Results showed that the amplitude of $[\text{Ca}^{2+}]_i$ transients was significantly lower in the TAC-vehicle group than in the sham groups, which was accompanied by a slower decay time constant (τ) (Figure 4C and 4D). These changes were also associated with a decrease in cell contractility in the TAC-vehicle group (Figure 4E). By contrast, cardiomyocytes obtained from TAC-paricalcitol mice showed similar values of τ and amplitude of $[\text{Ca}^{2+}]_i$ transients to those of the sham groups. Paricalcitol treatment also prevented the TAC-induced decrease in cell shortening (Figure 4E). To determine whether the impairment in the systolic Ca^{2+} release was related to changes in SR- Ca^{2+} load, we used caffeine administration to estimate the SR- Ca^{2+} load in representative cardiomyocytes of the 4 groups. As shown in Figure 4F, the amplitude of caffeine-evoked $[\text{Ca}^{2+}]_i$ transients was lower in the TAC groups than in the sham groups, and this was significantly prevented after 5 weeks of paricalcitol treatment. Decreased SR- Ca^{2+} load, together with slower time decay of $[\text{Ca}^{2+}]_i$ transients, would indicate a fault in SR- Ca^{2+} reuptake. Given that SR- Ca^{2+} ATPase (SERCA2a) plays a key role in SR- Ca^{2+} uptake, we next analysed SERCA2a activity (k_{SERCA2a}). Results showed that k_{SERCA2a} was significantly lower in the TAC group ($4.3 \pm 0.6 \text{ s}^{-1}$; $n=21$) than in the sham

group ($5.6 \pm 1.3 \text{ s}^{-1}$; n=16) or the sham paricalcitol group ($5.8 \pm 1.8 \text{ s}^{-1}$; n=11) ($p<0.05$), clearly indicating an impairment of SERCA2a function in cardiomyocytes from TAC hearts. Treatment of TAC mice with paricalcitol prevented this impairment ($5.4 \pm 1.7 \text{ s}^{-1}$; n=17). We next used RT-PCR to look for possible changes in the expression levels of *Atp2a2* (SERCA2a) and *Pln* (Phospholamban), which could account for the functional impairment in SR- Ca^{2+} load and re-uptake and the modulation by paricalcitol treatment. As shown in Figure 4G and 4H, expression of *Atp2a2* and *Pln* was significantly lower in the TAC group than in the sham group, and paricalcitol treatment prevented the decrease in expression of both genes. In addition, *Atp2a2/Pln* ratio was calculated and similar values between groups were obtained (Supporting information Figure S1). These results indicate that paricalcitol prevents Ca^{2+} mishandling in HF by maintaining both systolic Ca^{2+} release and physiological SR- Ca^{2+} load. Since depressed SR- Ca^{2+} load in HF is usually associated with an increase diastolic Ca^{2+} leak, we next analysed the frequency of Ca^{2+} sparks in all experimental groups. As expected, the analysis of the frequency of Ca^{2+} sparks normalised to SR Ca^{2+} load in quiescent cardiomyocytes showed a significant increase in the number of these events in the TAC group as compared with sham-operated group. By contrast, the frequency of Ca^{2+} sparks was significantly lower in TAC group treated with paricalcitol and was similar to that found in sham-Paricalcitol group (Supporting information, Figure S2). These data demonstrate that paricalcitol treatment significantly prevents the increase in diastolic Ca^{2+} leak observed in isolated cardiomyocytes from TAC hearts mice.

Paricalcitol prevents the transcriptional and structural development of fibrosis in established heart failure

Chronic pressure overload is commonly associated with myocardial fibrosis (Shimizu and Minamino, 2016). Accordingly, we next examined for fibrosis in heart tissue of the 4 experiment groups 9 weeks after surgery. Figure 5A and B show representative sirius red-stained images of perivascular (Figure 5A) and interstitial (Figure 5B) collagen. Histological and quantitative analysis showed that both parameters were significantly greater 9 weeks after TAC surgery (Figure 5C and 5D, respectively). Comparison of hearts from the TAC-vehicle and TAC-paricalcitol groups revealed that the development of perivascular (Figure 5C) and interstitial (Figure 5D) fibrosis was significantly attenuated in the latter.

Cardiac fibrosis is related to excessive synthesis and accumulation of the matrix protein collagen, and to the increased expression of plasminogen activator (PAI-1) (Takeshita et al.,

2004). Analysis of the expression of the pro-fibrotic genes *Serpine-1* (PAI-1), *Colla1* (Collagen-1) and *Col3a1* (Collagen-3) revealed that the expression of all was significantly higher in the TAC-vehicle group than in the sham groups (Figure 5E–G). Of note, cardiomyocytes from the TAC-paricalcitol group displayed mRNA values of the pro-fibrotic genes very similar to those of the sham groups. These results clearly indicate that paricalcitol treatment hinders, at the transcriptional and structural level, the development of cardiac fibrosis in an established model of HF.

Antihypertrophic effects of paricalcitol are related to inhibition of the calcineurin/NFAT pathway

Histological examination of hearts after 9 weeks of TAC corroborated the existence of LVH, with an increase in the size of the LV cavity (Figure 6A), and evident cardiomyocyte hypertrophy (Figure 6B). Paricalcitol treatment significantly attenuated TAC-induced LVH, both at the macroscopic and cellular levels. As shown in Figure 5C and Table 1, the HW/TL ratio was significantly greater in the TAC-vehicle group than in the sham groups, whereas this parameter was not affected in the TAC-paricalcitol group. In addition, quantitative analysis of cardiomyocyte surface area in the 4 groups showed that cells from the TAC-vehicle group were significantly larger than those from the sham groups (Figure 6 D and Table 1) and the TAC-induced increase in size was blocked by paricalcitol. The results from membrane capacitance analysis mirrored these findings (Table 1). To validate these results, we analysed the mRNA expression of atrial natriuretic peptide (ANP) (*Nppa*), a classic hypertrophic marker gene, in all groups, finding a pattern similar to that for the fibrosis marker genes (Figure 6E).

Finally, because the calcineurin/NFAT pathway is recognised as one of the most important signal transduction cascades underlying cardiac hypertrophy (Molkentin et al., 1998), we analysed the expression of the calcineurin/NFAT target gene *Rcan.1.4* (Regulator of calcineurin). As shown in Figure 6F, *Rcan.1.4* expression was significantly higher in the TAC-vehicle group than in the sham groups and, as anticipated, paricalcitol significantly attenuated its expression. This result suggests that the calcineurin/NFAT pathway is likely a target for the antihypertrophic action of paricalcitol.

Long QT, JT and TpTe intervals and reduced repolarising I_{K+} densities in mice with established heart failure are prevented by chronic paricalcitol administration.

LVH and HF are strongly associated with long QT intervals and repolarisation-related arrhythmogenic disorders. Accordingly, we measured ECG signals in mice 9 weeks after TAC surgery to study the effect of pressure overload on QT interval and the possible influence of paricalcitol on this parameter. Representative ECG recordings of QT interval measurements are shown in Figure 7A and mean QT intervals in the 4 groups are represented in Figure 7B. The results revealed that mean QT intervals were significantly longer in the TAC-vehicle group than in the sham groups. Notably, the mean QT intervals in the TAC-paricalcitol group were significantly shorter than in the TAC group and were similar to those in the sham groups. All of these changes occurred in the absence of alterations to the heart rate (Figure 7C). In addition to the QT interval, we analysed other parameters associated with ventricular electrocardiographic repolarization, namely, the JT interval (the interval between QRS end, J point, and the end of the T wave) and the TpTe interval (the interval from the peak to the end of the T wave). Both ECG parameters were increased in the TAC group and treatment with paricalcitol prevented their prolongation (Figure 7 D and 7E).

K^+ currents (I_{K+}) are important contributors to repolarisation in healthy myocardium and a reduction in the densities of I_{K+} have been associated with the acquired long QT syndrome seen in LVH and HF (Marionneau et al., 2008, Choy et al., 1997). Figure 8A shows representative recordings of total I_{K+} density in cardiomyocytes isolated from the 4 different groups of mice and Figure 8B shows mean IV curves for I_{K+} density. I_{K+} densities were significantly lower in the TAC-vehicle group than in the sham groups. By contrast, I_{K+} densities in the TAC-paricalcitol group were similar to those of the sham paricalcitol group. In the adult mouse ventricle, outward K^+ currents involved in the repolarisation phase, are composed of three components. Figures 8C, 8D and 8E show mean IV curves for I_{toF} , I_{kur} and I_{ss} densities, respectively, obtained in myocytes isolated from the 4 experimental groups. Mean values of all three components were significantly decreased in the TAC group for the three components as compared with sham or the sham-paricalcitol groups. One-way ANOVA of I_{toF} , I_{kur} and I_{ss} densities followed by Bonferroni's multiple comparisons test at +50 mV in the 4 experimental groups, showed that the treatment with paricalcitol significantly prevented the decrease of I_{toF} but not I_{kur} or I_{ss} (Figure 8F, 8G and 8H, respectively).

These results indicate that paricalcitol prevents QT, JT and TpTe interval prolongation induced by TAC, in the main part by preserving physiologic I_{K+} density, mostly I_{toF} in failing hearts.

DISCUSSION

Paricalcitol is a synthetic vitamin D3 analog that functions as a selective activator of VDR, and has been shown to reduce PTH levels with very low hypercalcemic and hyperphosphatemic secondary effects (Martin et al., 1998, Hervás Sánchez et al., 2011). The recommended dosage of paricalcitol in humans ranges from 0.04 to 0.24 $\mu\text{g/kg}$ administered as a bolus on alternate days (Robinson and Scott, 2005). In the present study, we used 0.3 $\mu\text{g/kg}$ paricalcitol by i.p. injection 3 times weekly (Monday, Wednesday and Friday) for 5 consecutive weeks. A large body of work demonstrates that the selective activation of VDR modulates, directly or indirectly, the transcriptional activity of hundreds of genes and modifies several enzymes and signalling pathways. Many of these pathways are involved in regulatory processes related to the parathyroid gland, gut and bone, but others are involved in non-classical actions of VDR, including those of potential relevance to cardiovascular diseases such as contractile function, hypertrophy, fibrosis, neurohormonal activation and inflammation (Lavie et al., 2011, Meredith and McManus, 2013, Norman and Powell, 2014, Andress, 2007).

Our results show that 5-weeks paricalcitol treatment in mice with established HF induced by TAC has a significant cardioprotective effect by halting the decline of left ventricular EF and the progression of pre-existing cardiac hypertrophy. Supporting our data, other authors have reported cardioprotective effects of paricalcitol on cardiac hypertrophy and development of HF in an experimental model of pressure overload in rats induced by a high-salt diet (Bae et al., 2011, Bodyak et al., 2007). Importantly, in the present study we comprehensively analysed the mechanisms involved in the beneficial effect of paricalcitol on the deleterious remodelling that occurs during HF development, and specifically focused on Ca^{2+} handling, myocardial fibrosis, cardiac hypertrophy and remodelling of repolarising K^{+} currents.

Cardiac pump function depends on cardiomyocyte contraction, which is activated by Ca^{2+} . Contraction is initiated by an action potential. The initial depolarization (mediated by Na^{+} channels) activates I_{CaL} , which triggers Ca^{2+} release from the SR, resulting in an increased

$[Ca^{2+}]_i$ that activates contraction. $[Ca^{2+}]_i$ must be reduced for relaxation to take place, and this occurs mainly by pumping Ca^{2+} to the SR *via* SERCA2a and across the plasma membrane *via* the sarcolemmal Na^+-Ca^{2+} exchanger (Bers, 2002). A decline in systolic Ca^{2+} release and SR- Ca^{2+} load is frequently reported in HF models, which also document a reduced expression and/or function of SERCA2a (Bers, 2006, Gómez-Hurtado et al., 2017). In our study, I_{CaL} density was not modified in any of the groups studied; however, ventricular cardiomyocytes isolated from failing hearts 9 weeks after TAC surgery showed diminished $[Ca^{2+}]_i$ transients with a slower time decay rate (τ) and a significant decrease in cell shortening. Furthermore, the caffeine-evoked $[Ca^{2+}]_i$ transients showed a decrease in SR- Ca^{2+} load. In this setting, paricalcitol treatment maintained the levels of $[Ca^{2+}]_i$ transient amplitude and cell shortening close to that observed in the sham group. In addition, SR- Ca^{2+} load was preserved. Moreover, paricalcitol treatment suppressed the decrease in the expression of both *Atp2a2* (SERCA2a) and *Pln* (phospholamban) observed in TAC hearts, which likely contributed to maintain SR- Ca^{2+} content, improving $[Ca^{2+}]_i$ transient amplitude and cell contractility. These data do not discard the possibility that posttranslational changes in PLN and/or SERCA2a might be involved in the observed effects.

Importantly, the prevention of the impairment in both systolic Ca^{2+} release and SR Ca^{2+} load induced by paricalcitol administration in the TAC group can also be due to a prevention of the increased diastolic Ca^{2+} leak associated with HF development. Indeed, our results support this idea, since paricalcitol administration significantly prevented the increased frequency of Ca^{2+} sparks in isolated cardiomyocytes obtained from hearts of TAC-induced mice. Along this line, paricalcitol significantly attenuated the impairment of Ca^{2+} handling and cardiac dysfunction in mice deleted for 1α -hydroxylase (Choudhury et al., 2014), which converts the inactive form of vitamin D₃ (25(OH)D₃) to the biological active form (1,25(OH)₂D₃).

Cardiac fibrosis is a distinguishing feature of pathological ventricular remodelling and can contribute to both systolic and diastolic cardiac dysfunction. It is characterised by myofibroblast differentiation and excessive synthesis and accumulation of matrix proteins, together with the induction of protease inhibitors, PAI-1 and tissue inhibitors of metalloproteinases (Kong et al., 2014, Weber et al., 1993, Takeshita et al., 2004). Indeed, it is well recognised that synthesis of type I and III collagens is markedly increased in the remodelling fibrotic heart irrespective of the aetiology of fibrosis (Weber et al., 1993, Mukherjee and Sen, 1993). Our histological and molecular analysis showed that paricalcitol treatment hindered the formation of perivascular and interstitial fibrosis 9 weeks after TAC

surgery. In accordance with our data, other authors have reported a role for paricalcitol in reducing fibrosis and remodelling in the myocardium (Meredith and McManus, 2013, Meems et al., 2012, Gardner et al., 2013).

The CMRI study also showed that paricalcitol had a significant effect in preventing the progression of pre-existing cardiac hypertrophy, as revealed by analysis of the HW/TL ratio and ventricular cardiomyocyte size. Similarly, the TAC-induced increase in the expression of the hypertrophic gene marker *Nppa* (ANP) was significantly blunted by paricalcitol, further supporting its anti-hypertrophic activity. Indeed, anti-hypertrophic effects of paricalcitol have been described in other experimental models of HF (Bae et al., 2011, Kong et al., 2014, Bodyak et al., 2007) and in uremic rats (Freundlich et al., 2014). The mechanisms underlying the anti-hypertrophic effects of the VDR pathway have been investigated in cardiomyocyte-specific VDR knockout mice, which exhibit significant cardiac hypertrophy and activation of the fetal gene program (Chen et al., 2011). Importantly, it has been reported that the anti-hypertrophic activity of paricalcitol is lost in these mice after treatment with angiotensin II, supporting that the direct action of paricalcitol on cardiomyocytes is independent of hemodynamic effects (Gardner et al., 2013, Chen and Gardner, 2013). Our results clearly demonstrate an increase of diastolic Ca^{2+} leak in failing (TAC) mice. Moreover, the sustained elevation of the cytosolic calcium that occurs in HF has been proven to activate calcineurin-NFAT signalling. Dephosphorylation of NFAT by calcineurin allows for NFAT to enter the nucleus, to promote the expression of genes involved in structural cardiac remodelling (Olson and Williams, 2000, Wilkins and Molkentin, 2004). Paricalcitol treatment prevented the impairment in diastolic Ca^{2+} release and SR- Ca^{2+} load, thus reducing the cytosolic Ca^{2+} concentration, which counteracts the activation of calcineurin/NFAT pathway. Moreover, results from gene expression array analysis of isolated ventricular myocytes of cardiomyocyte-specific VDR knockout mice showed that the expression of modulatory calcineurin inhibitory protein 1 (MCIP1 or Rcan1.4) was upregulated 2-fold as compared with control cells (Chen et al., 2011). RCANs are a family of proteins that can bind directly to the catalytic subunit of calcineurin and inhibit its activity. RCAN 1.4 works as an endogenous feedback inhibitor, protecting cells from uncontrolled calcineurin activity. The calcineurin/NFAT/Rcan1.4 cascade has been linked to the development of pathological hypertrophy in several experimental models of pressure overload (Zou et al., 2001, Wilkins et al., 2004, Diedrichs et al., 2004) and also in human HF (Lim and Molkentin, 1999, Diedrichs et al., 2004). In the present study, we found that the increase in *Rcan1.4* mRNA expression in

hypertrophied hearts from TAC mice was blunted by paricalcitol treatment, suggesting that the VDR-dependent antihypertrophic activity of paricalcitol is linked to the negative modulation of the calcineurin/NFAT/*Rcan1.4* pathway. A similar inhibition of the NFAT target gene *Rcan1.4* associated with reduced cardiac hypertrophy was recently reported in paricalcitol-treated uremic rats (Czaya et al., 2019).

LVH and HF are associated with QT prolongation and increased susceptibility for ventricular arrhythmias (Nass et al., 2008, Tomaselli and Marbán, 1999). Indeed, about 50% of the mortality in patients with HF is reported to be associated with sudden cardiac death, which is often related to malignant ventricular arrhythmias (Nass et al., 2008, Tomaselli et al., 1994). In addition, prolonged TpTe interval has been associated with increased risk of sudden cardiac death in patients (Panikkath et al., 2011). Therefore, in addition to the QT interval, we examined other electrocardiographic parameters associated with ventricular repolarization, finding that the QT, JT and TpTe intervals were significantly prolonged in TAC-operated mice, whereas TAC-induced mice receiving paricalcitol showed a significant decrease in the duration of the three intervals. The mechanism for prolongation of ventricular repolarization in HF involves the development of adverse electrophysiological remodelling including downregulation of K^+ currents responsible for repolarization of the action potential (Nattel et al., 2007). Using patch-clamp experiments we found that the density of I_{K^+} , I_{tof} , I_{kur} and I_{ss} were significantly lower in myocytes isolated from TAC mice than in sham or sham paricalcitol groups. Treatment of TAC mice with paricalcitol prevented this decrease mainly for I_{K^+} and I_{tof} . A reduction in I_{tof} density has been reported in animal models of HF (Gómez-Hurtado et al., 2017, Wang et al., 2007) and in humans (Beuckelmann et al., 1993, Näbauer et al., 1993). Our results thus establish that paricalcitol reduces QT, JT and Tp Te interval prolongation associated with LVH and HF by preventing deleterious electrophysiological remodelling. Therefore, through this mechanism, paricalcitol might attenuate the vulnerability to LVH/HF-associated ventricular arrhythmias.

In conclusion, we provide the first demonstration that paricalcitol, a drug used for the treatment of secondary hyperparathyroidism, prevents the progression of established HF by alleviating LVH, cardiac fibrosis and adverse electrophysiological and Ca^{2+} handling remodelling. Our results suggest that paricalcitol might emerge as a potential therapeutic option in the treatment of HF.

Author contributions

MT and LM-N, performed most of the experiments, AV-B and MF-V helped with Ca^{2+} handling experiments, EL contributed to CMRI analysis, JAN-G and G.R-H performed ECG studies, PP helped with RT-PCR studies, MJG-P, helped with TAC surgery, G.R-H and MF-V contributed to the critical interpretation of data, MF-V and CD performed some electrophysiological and Ca^{2+} handling experiments, conceived the hypothesis, supervised the project, reviewed the data and wrote the manuscript. All the authors critically analysed the manuscript and approved its final version for publication.

Acknowledgments

We are grateful to María Gracia Gonzalez-Bueno for her technical assistance and Dr. Kenneth McCreath for English editing. The authors acknowledge the facilities and scientific technical assistance of Dr. Teresa Vallejo and the Immunohistochemistry Unit, IdiPaz. This work was supported by the Spanish Ministry of Economy and Competitiveness (SAF2014-57190R, SAF2017-84777-R), ISCIII (PI17/01093 and PI17/01344), European Regional Development Fund (FEDER), Sociedad Española de Cardiología (SEC), and CIBER-CV, a network funded by ISCIII. MF-V is a Miguel Servet II researcher of ISCIII (MSII16/00047 Carlos III Health Institute). GR-H is a Miguel Servet I researcher of ISCIII (CP15/00129 Carlos III Health Institute). MT is a predoctoral fellow of the Spanish Ministry of Science, Innovation and Universities (FPU-17/06135).

Disclosure statement

The authors have nothing to disclose

Declaration of transparency and scientific rigour

This Declaration acknowledges that this paper adheres to the principles for transparent reporting and scientific rigour of preclinical research as stated in the BJP guidelines for Design & Analysis, and Animal Experimentation, and as recommended by funding agencies, publishers and other organisations engaged with supporting research.

REFERENCES

- ALEXANDER, SPH., DAVENPORT, AP., KELLY, E., MARRION, N., PETERS, JA., BENSON, HE. ET AL. 2015a. The Concise Guide to PHARMACOLOGY 2015/16: Voltage-gated ion channels. *Br J Pharmacol* 172: 5904–37.
- ALEXANDER, SPH., DAVENPORT, AP., KELLY, E., MARRION, N., PETERS, JA., BENSON, HE. ET AL. 2015b. The Concise Guide to PHARMACOLOGY 2015/16: Nuclear hormone receptors. *Br J Pharmacol* 172: 5956–76.
- ANDRESS, D. 2007. Nonclassical aspects of differential vitamin D receptor activation: implications for survival in patients with chronic kidney disease. *Drugs*, 67, 1999–2012.
- BAE, S., YALAMARTI, B., KE, Q., CHOUDHURY, S., YU, H., KARUMANCHI, S. A., KROEGER, P., THADHANI, R. & KANG, P. M. 2011. Preventing progression of cardiac hypertrophy and development of heart failure by paricalcitol therapy in rats. *Cardiovasc Res*, 91, 632–9.
- BERS, D. M. 2002. Cardiac excitation-contraction coupling. *Nature*, 415, 198–205.
- BERS, D. M. 2006. Altered cardiac myocyte Ca regulation in heart failure. *Physiology (Bethesda)*, 21, 380–7.
- BEUCKELMANN, D. J., NÄBAUER, M. & ERDMANN, E. 1993. Alterations of K⁺ currents in isolated human ventricular myocytes from patients with terminal heart failure. *Circ Res*, 73, 379–85.
- BODE, E. F., BRISTON, S. J., OVEREND, C. L., O'NEILL, S. C., TRAFFORD, A. W. & EISNER, D. A. 2011. Changes of SERCA activity have only modest effects on sarcoplasmic reticulum Ca²⁺ content in rat ventricular myocytes. *J Physiol*, 589, 4723–9.
- BODYAK, N., AYUS, J. C., ACHINGER, S., SHIVALINGAPPA, V., KE, Q., CHEN, Y. S., RIGOR, D. L., STILLMAN, I., TAMEZ, H., KROEGER, P. E., WU-WONG, R. R., KARUMANCHI, S. A., THADHANI, R. & KANG, P. M. 2007. Activated vitamin D attenuates left ventricular abnormalities induced by dietary sodium in Dahl salt-sensitive animals. *Proc Natl Acad Sci U S A*, 104, 16810–5.
- CHEN, S. & GARDNER, D. G. 2013. Liganded vitamin D receptor displays anti-hypertrophic activity in the murine heart. *J Steroid Biochem Mol Biol*, 136, 150–5.
- CHEN, S., LAW, C. S., GRIGSBY, C. L., OLSEN, K., HONG, T. T., ZHANG, Y., YEGHIAZARIANS, Y. & GARDNER, D. G. 2011. Cardiomyocyte-specific deletion of the vitamin D receptor gene results in cardiac hypertrophy. *Circulation*, 124, 1838–47.
- CHOUDHURY, S., BAE, S., KE, Q., LEE, J. Y., SINGH, S. S., ST-ARNAUD, R., MONTE, F. D. & KANG, P. M. 2014. Abnormal calcium handling and exaggerated cardiac dysfunction in mice with defective vitamin d signaling. *PLoS One*, 9, e108382.
- CHOY, A. M., LANG, C. C., CHOMSKY, D. M., RAYOS, G. H., WILSON, J. R. & RODEN, D. M. 1997. Normalization of acquired QT prolongation in humans by intravenous potassium. *Circulation*, 96, 2149–54.
- CURTIS, M. J., ASHTON, J. C., MOON, L. D. F. & AHLUWALIA, A. 2018. Clarification of the basis for the selection of requirements for publication in the British Journal of Pharmacology. *Br J Pharmacol*, 175, 3633–3635.
- CZAYA, B., SEEHERUNVONG, W., SINGH, S., YANUCIL, C., RUIZ, P., QUIROZ, Y., GRABNER, A., KATSOUFIS, C., SWAMINATHAN, S., ABITBOL, C., RODRIGUEZ-ITURBE, B., FAUL, C. & FREUNDLICH, M. 2019. Cardioprotective Effects of Paricalcitol Alone and in Combination With FGF23 Receptor Inhibition in Chronic Renal Failure: Experimental and Clinical Studies. *Am J Hypertens*, 32, 34–44.

- DELGADO, C., RUIZ-HURTADO, G., GOMEZ-HURTADO, N., GONZALEZ-RAMOS, S., RUEDA, A., BENITO, G., PRIETO, P., ZARAGOZA, C., DELICADO, E. G., PEREZ-SEN, R., MIRAS-PORTUGAL, M. T., NUNEZ, G., BOSCA, L. & FERNANDEZ-VELASCO, M. 2015. NOD1, a new player in cardiac function and calcium handling. *Cardiovascular Research*, 106, 375-386.
- DIEDRICH, H., CHI, M., BOELCK, B., MEHLHORN, U., MEHLHORN, U. & SCHWINGER, R. H. 2004. Increased regulatory activity of the calcineurin/NFAT pathway in human heart failure. *Eur J Heart Fail*, 6, 3-9.
- FREUNDLICH, M., LI, Y. C., QUIROZ, Y., BRAVO, Y., SEEHERUNVONG, W., FAUL, C., WEISINGER, J. R. & RODRIGUEZ-ITURBE, B. 2014. Paricalcitol downregulates myocardial renin-angiotensin and fibroblast growth factor expression and attenuates cardiac hypertrophy in uremic rats. *Am J Hypertens*, 27, 720-6.
- GARDNER, D. G., CHEN, S. & GLENN, D. J. 2013. Vitamin D and the heart. *Am J Physiol Regul Integr Comp Physiol*, 305, R969-77.
- GÓMEZ-HURTADO, N., DOMÍNGUEZ-RODRÍGUEZ, A., MATEO, P., FERNÁNDEZ-VELASCO, M., VAL-BLASCO, A., AIZPÚN, R., SABOURIN, J., GÓMEZ, A. M., BENITAH, J. P. & DELGADO, C. 2017. Beneficial effects of leptin treatment in a setting of cardiac dysfunction induced by transverse aortic constriction in mouse. *J Physiol*, 595, 4227-4243.
- HERVÁS SÁNCHEZ, J. G., PRADOS GARRIDO, M. D., POLO MOYANO, A. & CEREZO MORALES, S. 2011. Effectiveness of treatment with oral paricalcitol in patients with pre-dialysis chronic kidney disease. *Nefrologia*, 31, 697-706.
- HEUSCH, G., LIBBY, P., GERSH, B., YELLON, D., BÖHM, M., LOPASCHUK, G. & OPIE, L. 2014. Cardiovascular remodelling in coronary artery disease and heart failure. *Lancet*, 383, 1933-43.
- KILKENNY, C., BROWNE, W., CUTHILL, I. C., EMERSON, M., ALTMAN, D. G. & GROUP, N. R. R. G. W. 2010. Animal research: reporting in vivo experiments: the ARRIVE guidelines. *Br J Pharmacol*, 160, 1577-9.
- KONG, P., CHRISTIA, P. & FRANGOIANNIS, N. G. 2014. The pathogenesis of cardiac fibrosis. *Cell Mol Life Sci*, 71, 549-74.
- LAVIE, C. J., LEE, J. H. & MILANI, R. V. 2011. Vitamin D and cardiovascular disease will it live up to its hype? *J Am Coll Cardiol*, 58, 1547-56.
- LIM, H. W. & MOKKENTIN, J. D. 1999. Calcineurin and human heart failure. *Nat Med*, 5, 246-7.
- MARIONNEAU, C., BRUNET, S., FLAGG, T. P., PILGRAM, T. K., DEMOLOMBE, S. & NERBONNE, J. M. 2008. Distinct cellular and molecular mechanisms underlie functional remodeling of repolarizing K⁺ currents with left ventricular hypertrophy. *Circ Res*, 102, 1406-15.
- MARTIN, K. J., GONZÁLEZ, E. A., GELLENS, M., HAMM, L. L., ABOUD, H. & LINDBERG, J. 1998. 19-Nor-1- α -25-dihydroxyvitamin D₂ (Paricalcitol) safely and effectively reduces the levels of intact parathyroid hormone in patients on hemodialysis. *J Am Soc Nephrol*, 9, 1427-32.
- MCGRATH, J. C., DRUMMOND, G. B., MCLACHLAN, E. M., KILKENNY, C. & WAINWRIGHT, C. L. 2010. Guidelines for reporting experiments involving animals: the ARRIVE guidelines. *Br J Pharmacol*, 160, 1573-6.
- MEEMS, L. M., CANNON, M. V., MAHMUD, H., VOORS, A. A., VAN GILST, W. H., SILLJÉ, H. H., RUIFROK, W. P. & DE BOER, R. A. 2012. The vitamin D receptor activator paricalcitol prevents fibrosis and diastolic dysfunction in a murine model of pressure overload. *J Steroid Biochem Mol Biol*, 132, 282-9.

- MEREDITH, A. J. & MCMANUS, B. M. 2013. Vitamin D in heart failure. *J Card Fail*, 19, 692-711.
- MOLKENTIN, J. D., LU, J. R., ANTOS, C. L., MARKHAM, B., RICHARDSON, J., ROBBINS, J., GRANT, S. R. & OLSON, E. N. 1998. A calcineurin-dependent transcriptional pathway for cardiac hypertrophy. *Cell*, 93, 215-28.
- MUKHERJEE, D. & SEN, S. 1993. Alteration of cardiac collagen phenotypes in hypertensive hypertrophy: role of blood pressure. *J Mol Cell Cardiol*, 25, 185-96.
- NABEEBACCUS, A., ZHENG, S. & SHAH, A. M. 2016. Heart failure-potential new targets for therapy. *Br Med Bull*, 119, 99-110.
- NASS, R. D., AIBA, T., TOMASELLI, G. F. & AKAR, F. G. 2008. Mechanisms of disease: ion channel remodeling in the failing ventricle. *Nat Clin Pract Cardiovasc Med*, 5, 196-207.
- NATTEL, S., MAGUY, A., LE BOUTER, S. & YEH, Y. H. 2007. Arrhythmogenic ion-channel remodeling in the heart: heart failure, myocardial infarction, and atrial fibrillation. *Physiol Rev*, 87, 425-56.
- NORMAN, P. E. & POWELL, J. T. 2014. Vitamin D and cardiovascular disease. *Circ Res*, 114, 379-93.
- NÄBAUER, M., BEUCKELMANN, D. J. & ERDMANN, E. 1993. Characteristics of transient outward current in human ventricular myocytes from patients with terminal heart failure. *Circ Res*, 73, 386-94.
- OLSON, E. N. & WILLIAMS, R. S. 2000. Calcineurin signaling and muscle remodeling. *Cell*, 101, 689-92.
- OWENS, A. T., BROZENA, S. C. & JESSUP, M. 2016. New Management Strategies in Heart Failure. *Circ Res*, 118, 480-95.
- PANIKKATH, R., REINIER, K., UY-EVANADO, A., TEODORESCU, C., HATTENHAUER, J., MARIANI, R., GUNSON, K., JUI, J. & CHUGH, S. S. 2011. Prolonged Tpeak-to-tend interval on the resting ECG is associated with increased risk of sudden cardiac death. *Circ Arrhythm Electrophysiol*, 4, 441-7.
- PONIKOWSKI, P., ANKER, S. D., ALHABIB, K. F., COWIE, M. R., FORCE, T. L., HU, S., JAARSMA, T., KRUM, H., RASTOGI, V., ROHDE, L. E., SAMAL, U. C., SHIMOKAWA, H., BUDI SISWANTO, B., SLIWA, K. & FILIPPATOS, G. 2014. Heart failure: preventing disease and death worldwide. *ESC Heart Fail*, 1, 4-25.
- ROBINSON, D. M. & SCOTT, L. J. 2005. Paricalcitol: a review of its use in the management of secondary hyperparathyroidism. *Drugs*, 65, 559-76.
- ROCKMAN, H. A., ROSS, R. S., HARRIS, A. N., KNOWLTON, K. U., STEINHELPER, M. E., FIELD, L. J., ROSS, J. & CHIEN, K. R. 1991. Segregation of atrial-specific and inducible expression of an atrial natriuretic factor transgene in an in vivo murine model of cardiac hypertrophy. *Proc Natl Acad Sci U S A*, 88, 8277-81.
- RUIZ-HURTADO, G., LI, L., FERNÁNDEZ-VELASCO, M., RUEDA, A., LEFEBVRE, F., WANG, Y., MATEO, P., CASSAN, C., GELLEN, B., BENITAH, J. P. & GÓMEZ, A. M. 2015. Reconciling depressed Ca²⁺ sparks occurrence with enhanced RyR2 activity in failing mice cardiomyocytes. *J Gen Physiol*, 146, 295-306.
- SAVARESE, G. & LUND, L. H. 2017. Global Public Health Burden of Heart Failure. *Card Fail Rev*, 3, 7-11.
- SHIMIZU, I. & MINAMINO, T. 2016. Physiological and pathological cardiac hypertrophy. *J Mol Cell Cardiol*, 97, 245-62.
- SOUTHAN, C., SHARMAN, J. L., BENSON, H. E., FACCENDA, E., PAWSON, A. J., ALEXANDER, S. P. ET AL. 2016. The IUPHAR/BPS Guide to PHARMACOLOGY in 2016: towards curated quantitative interactions between 1300 protein targets and 6000 ligands. *Nucl Acids Res* 44: D1054-1068.

- TAKESHITA, K., HAYASHI, M., IINO, S., KONDO, T., INDEN, Y., IWASE, M., KOJIMA, T., HIRAI, M., ITO, M., LOSKUTOFF, D. J., SAITO, H., MUROHARA, T. & YAMAMOTO, K. 2004. Increased expression of plasminogen activator inhibitor-1 in cardiomyocytes contributes to cardiac fibrosis after myocardial infarction. *Am J Pathol*, 164, 449-56.
- TAMARGO, J., CABALLERO, R. & DELPÓN, E. 2018. New drugs in preclinical and early stage clinical development in the treatment of heart failure. *Expert Opin Investig Drugs*, 1-21.
- TAMAYO, M., MARTIN-NUNES, L., VAL-BLASCO, A., PIEDRAS, M. J., LARRIBA, M. J., GÓMEZ-HURTADO, N., FERNÁNDEZ-VELASCO, M. & DELGADO, C. 2018. Calcitriol, the Bioactive Metabolite of Vitamin D, Increases Ventricular K. *Front Physiol*, 9, 1186.
- TOMASELLI, G. F., BEUCKELMANN, D. J., CALKINS, H. G., BERGER, R. D., KESSLER, P. D., LAWRENCE, J. H., KASS, D., FELDMAN, A. M. & MARBAN, E. 1994. Sudden cardiac death in heart failure. The role of abnormal repolarization. *Circulation*, 90, 2534-9.
- TOMASELLI, G. F. & MARBÁN, E. 1999. Electrophysiological remodeling in hypertrophy and heart failure. *Cardiovasc Res*, 42, 270-83.
- VAL-BLASCO, A., PIEDRAS, M. J. G. M., RUIZ-HURTADO, G., SUAREZ, N., PRIETO, P., GONZALEZ-RAMOS, S., GOMEZ-HURTADO, N., DELGADO, C., PEREIRA, L., BENITO, G., ZARAGOZA, C., DOMENECH, N., GENEROSA CRESPO-LEIRO, M., VASQUEZ-ECHEVERRI, D., NUNEZ, G., LOPEZ-COLLAZO, E., BOSCA, L. & FERNANDEZ-VELASCO, M. 2017. Role of NOD1 in Heart Failure Progression via Regulation of Ca²⁺ Handling. *Journal of the American College of Cardiology*, 69, 423-433.
- WANG, Y., CHENG, J., CHEN, G., ROB, F., NASEEM, R. H., NGUYEN, L., JOHNSTONE, J. L. & HILL, J. A. 2007. Remodeling of outward K⁺ currents in pressure-overload heart failure. *J Cardiovasc Electrophysiol*, 18, 869-75.
- WEBER, K. T., BRILLA, C. G. & JANICKI, J. S. 1993. Myocardial fibrosis: functional significance and regulatory factors. *Cardiovasc Res*, 27, 341-8.
- WILKINS, B. J., DAI, Y. S., BUENO, O. F., PARSONS, S. A., XU, J., PLANK, D. M., JONES, F., KIMBALL, T. R. & MOLKENTIN, J. D. 2004. Calcineurin/NFAT coupling participates in pathological, but not physiological, cardiac hypertrophy. *Circ Res*, 94, 110-8.
- WILKINS, B. J. & MOLKENTIN, J. D. 2004. Calcium-calcineurin signaling in the regulation of cardiac hypertrophy. *Biochem Biophys Res Commun*, 322, 1178-91.
- ZOU, Y., HIROI, Y., UOZUMI, H., TAKIMOTO, E., TOKO, H., ZHU, W., KUDOH, S., MIZUKAMI, M., SHIMOYAMA, M., SHIBASAKI, F., NAGAI, R., YAZAKI, Y. & KOMURO, I. 2001. Calcineurin plays a critical role in the development of pressure overload-induced cardiac hypertrophy. *Circulation*, 104, 97-101.

Table 1: Macroscopic parameters, cell capacitance, and serum analysis from each experimental group 9 weeks after surgery. Values are expressed as Mean \pm SEM. #p<0.05 vs Sham-vehicle. & p<0.05 vs TAC-vehicle. PTH = parathyroid hormone. HW = heart weight. TL = tibia length. N = number of mice. n = number of independent cardiomyocytes.

	Sham		TAC	
	Vehicle	Paricalcitol	Vehicle	Paricalcitol
Ca²⁺ [mg dL⁻¹]	12.5 \pm 0.6 (N= 16)	11.4 \pm 0.6 (N= 8)	11.0 \pm 0.6 (N= 15)	12.4 \pm 0.5 (N= 14)
PTH [pg mL⁻¹]	145.2 \pm 17.4 (N= 12)	56.0 \pm 6.9 [#] (N= 7)	123.0 \pm 12.4 (N= 14)	52.8 \pm 3.4 ^{&} (N= 11)
P_i [mg dL⁻¹]	8.6 \pm 0.5 (N= 15)	6.8 \pm 0.7 (N= 9)	7.1 \pm 0.7 (N= 15)	8.0 \pm 0.5 (N= 15)
Ratio (HW TL⁻¹)	9.9 \pm 0.3 (N= 13)	9.9 \pm 0.3 (N= 12)	15.2 \pm 1.0 [#] (N= 15)	12.1 \pm 0.6 ^{&} (N= 14)
HW (mg)	174.6 \pm 5.9 (N= 13)	180.3 \pm 7.1 (N= 12)	273.6 \pm 18.3 [#] (N= 15)	187.7 \pm 21.9 ^{&} (N= 14)
TL (mm)	17.6 \pm 0.2 (N= 13)	18.2 \pm 0.2 (N= 12)	17.9 \pm 0.2 [#] (N= 15)	17.7 \pm 0.2 ^{&} (N= 14)
Cell area (μm^2)	3251 \pm 121.0 (N=6; n=72)	3422 \pm 159.1 (N=5; n=45)	4555 \pm 167.4 [#] (N=6; n=78)	3941 \pm 177.1 ^{&} (N=6; n=56)
Capacitance (pF)	186.3 \pm 16.8 (N=5; n=13)	189.7 \pm 15.8 (N=5; n=10)	375.9 \pm 39.6 [#] (N=5; n=12)	236.2 \pm 16.8 ^{&} (N=5; n=15)

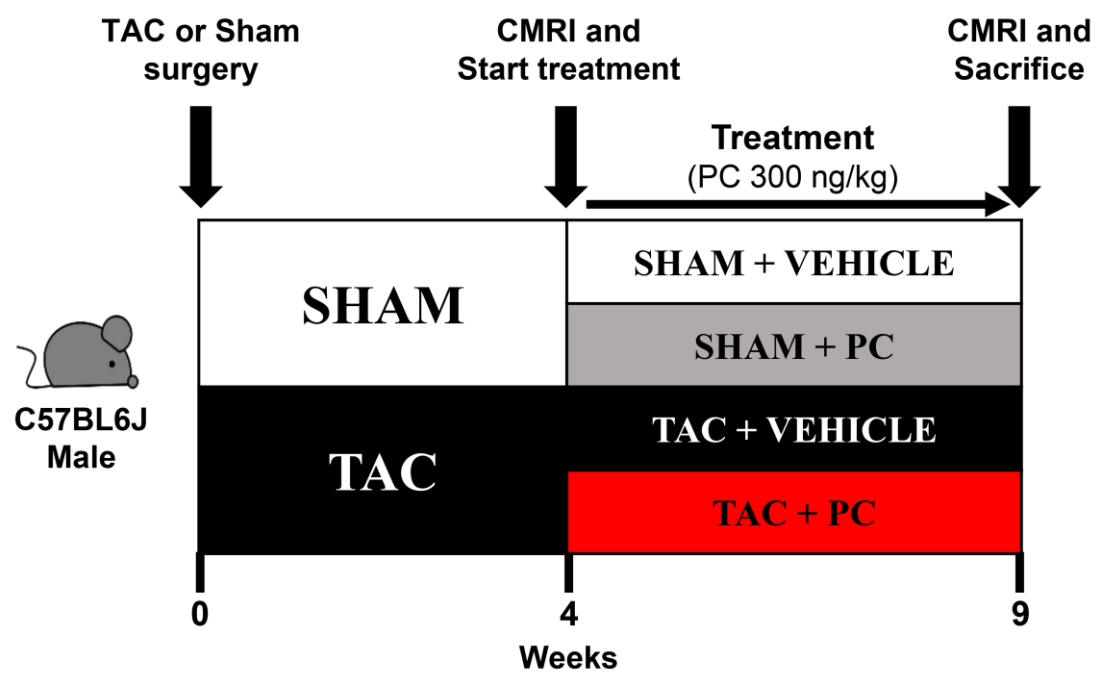


Figure 1. Schematic diagram of experimental design.

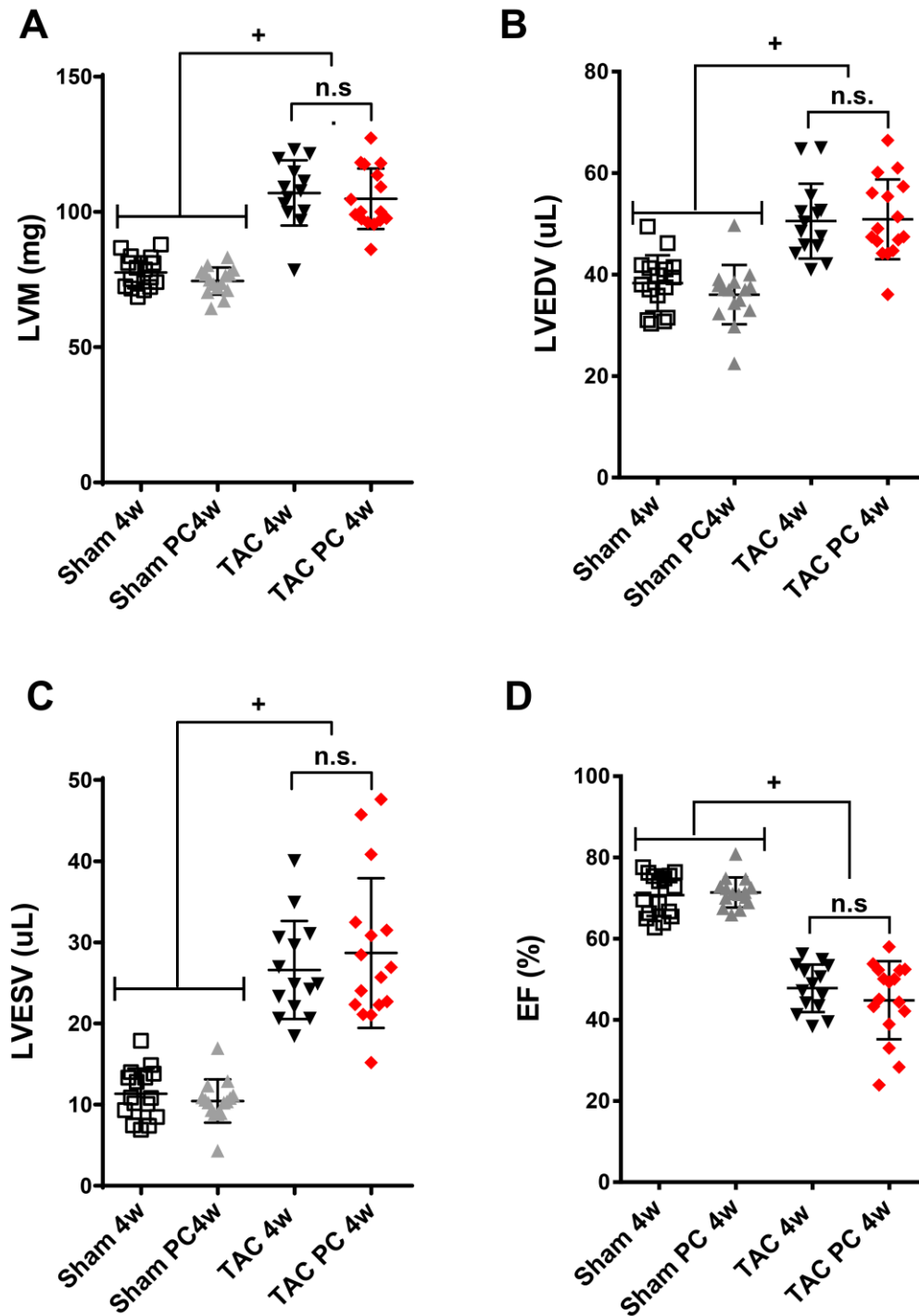


Figure 2. Stage of the disease before paricalcitol treatment analysed by cardiac magnetic resonance imaging (CMRI). (A) Left ventricular mass (LVM), (B) left ventricular end diastolic volume (LVEDV), (C) Left ventricular end systolic volume (LVESV), (D) Ejection fraction (EF). There were no differences between the TAC and TAC PC groups in any parameter before the treatment was initiated. Sham (N=16), sham PC (N=15), TAC (N=14) and TAC PC (N=16). Data expressed as mean±SD. +p<0.05 both groups Sham vs. both groups TAC. n.s. = non-significant. N = number of mice. PC = paricalcitol.

A

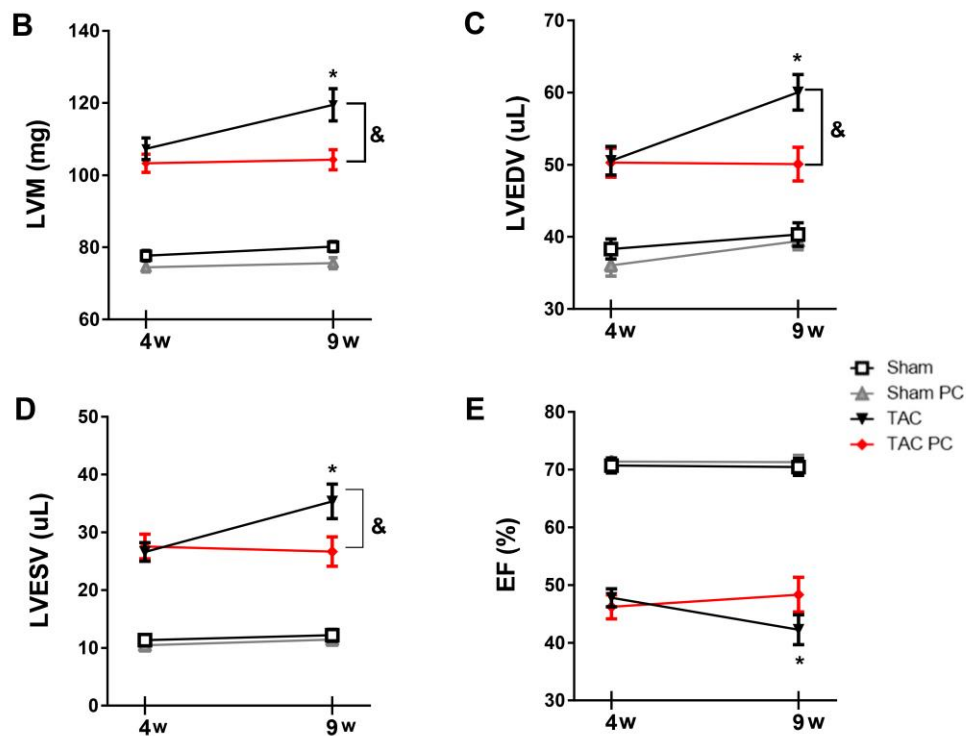
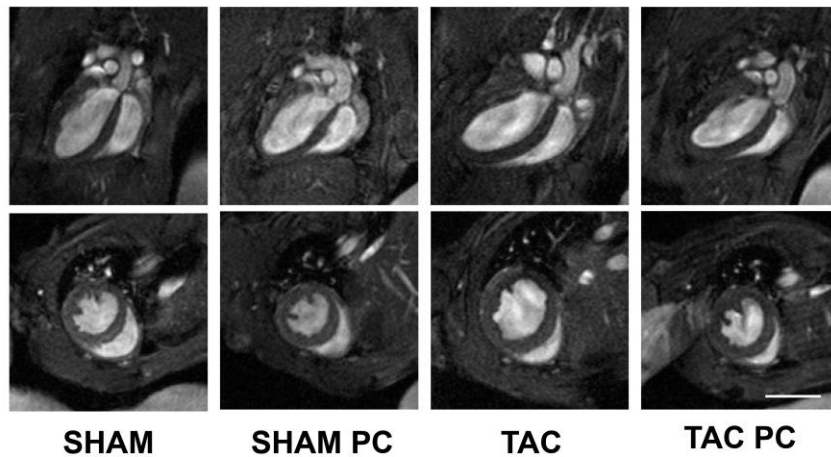


Figure 3. Paricalcitol blocks pathological progression of heart failure. (A) Representative cardiac magnetic resonance (CMR) images of mouse hearts at the end of diastole. Top, 4-chamber long-axis views; *bottom*, 2-chamber short-axis views. (B) CMR analysis of left ventricular mass (LVM), (C) left ventricular end diastolic volume (LVEDV), (D) left ventricular end systolic volume (LVESV) and (E) ejection fraction (EF). Groups are sham (N=16), sham PC (N=15), TAC (N=14) and TAC PC (N=16). Data expressed as mean±SEM. *p<0.05 vs TAC 4w. &p<0.05 TAC 9w vs. TAC PC 9w. Each TAC group was statistically different from each sham group p<0.05. N = number of mice. PC = paricalcitol. Scale bar represents 5 mm.

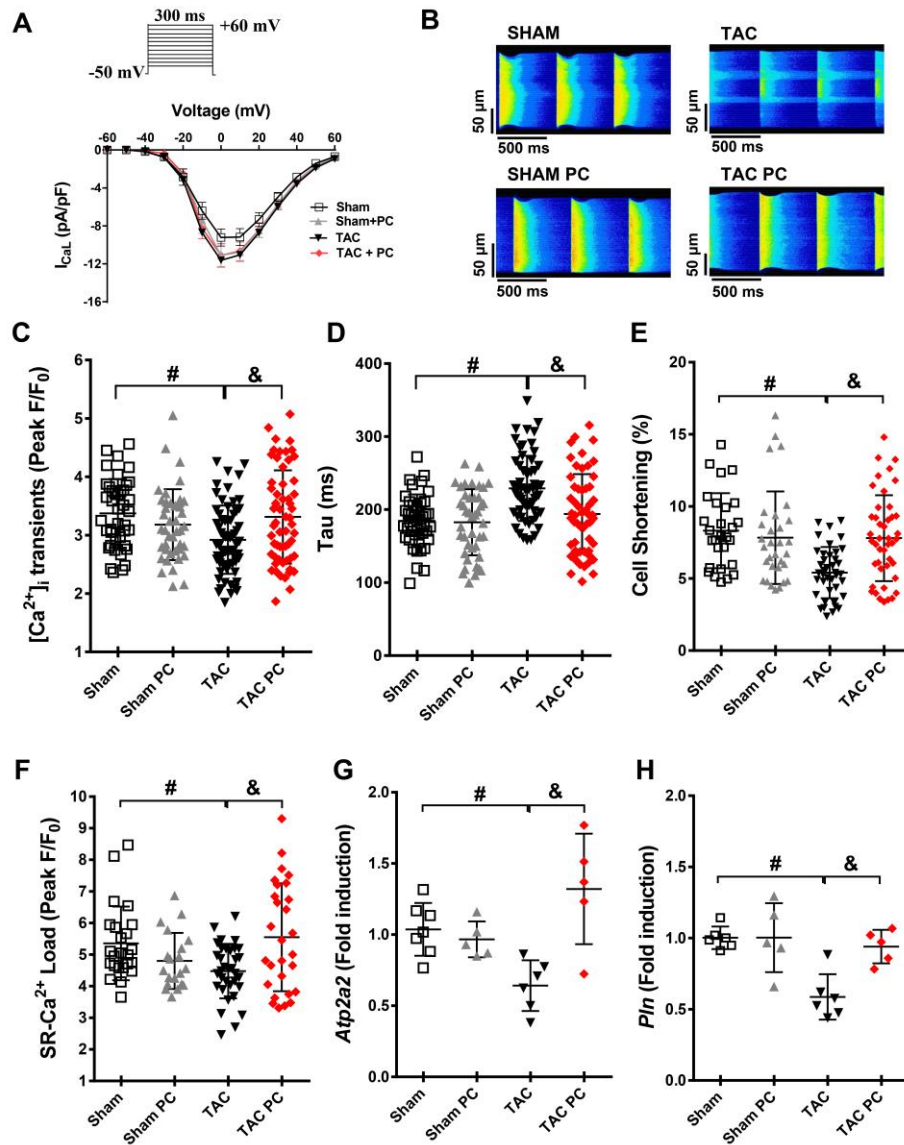


Figure 4. Paricalcitol treatment attenuates $[Ca^{2+}]_i$ mishandling in isolated myocytes from hearts after 9 weeks of TAC. (A) Current-voltage curves for I_{CaL} density obtained in myocytes isolated from sham (n=13, N=4), sham PC (n=10, N=4), TAC (n=12, N=4) and TAC PC (n=15, N=4) groups. The upper panel shows the protocol used to elicit I_{CaL} . (B) Representative line-scan confocal images of transients stimulated to 2 Hz in cells from sham, sham PC, TAC and TAC PC groups. (C) Mean values of peak of fluorescence $[Ca^{2+}]_i$ transients (Peak F/F_0), (D) decay time constant (tau) and (E) cell shortening in sham (n=42, N=6), sham PC (n=42, N=5), TAC (n=62, N=6) and TAC PC (n=58, N=6) groups. (F) Mean values of amplitude SR- Ca^{2+} load (Peak F/F_0) are shown in sham (n=24, N=6) sham PC (n=26, N=5), TAC (n=34, N=6) and TAC PC (n=29, N=6) groups. (G) Paricalcitol treatment increases mRNA expression of *Atp2a2* (SERCA2a) and (H) *Pln* (Phospholamban) 9 weeks after TAC surgery. Sham (N=7), Sham PC (N=5), TAC (N=7) and TAC PC (N=6). Data expressed as mean \pm SEM in panel A and mean \pm SD in panels C-H. #p<0.05 Sham vs. TAC &p<0.05 TAC vs. TAC PC. Sham vs. Sham PC groups were not significantly different. N = number of mice; n = number of independent cardiomyocytes. PC = paricalcitol.

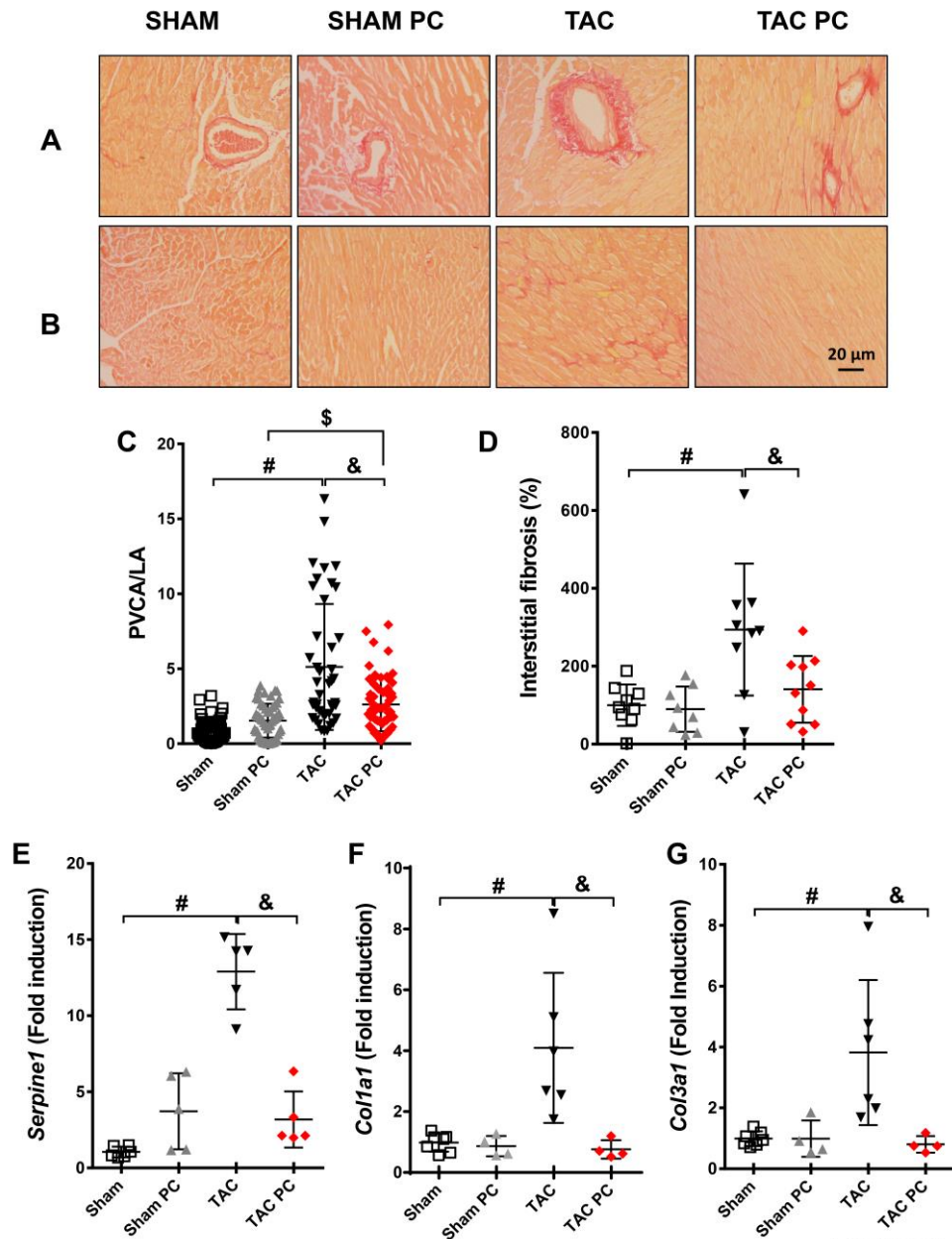


Figure 5. Paricalcitol treatment inhibits the progression of both perivascular and interstitial cardiac fibrosis by preventing the increased expression of *serpine1*, *Colla1* and *Col3a1*. (A, B) Representative images of sirius red staining showing perivascular (A) and interstitial (B) fibrosis from each experimental group 9 weeks after the surgery. (C) Paricalcitol treatment attenuates the increase of perivascular fibrosis (normalised by luminal area). Groups are sham (n=49, N=9), sham PC (n=57, N=9), TAC (n=43, N=9) and TAC PC (n=60, N=10). (D) Interstitial fibrosis is also diminished by paricalcitol treatment. Groups are sham (N=9), sham PC (N=9), TAC (N=9) and TAC PC (N=10). (E,F,G) Real-time PCR analysis of mRNA expression of *serpine1*, *colla1* and *col3a1*. Groups are sham (N=7), sham PC (N=5), TAC (N=7) and TAC PC (N=6). Data expressed as mean \pm SD. #p<0.05 sham vs TAC; &p<0.05 TAC vs TAC PC. \$p<0.05 sham PC vs. TAC PC. Sham vs. Sham PC groups were not significantly different PVCA = Perivascular collagen area. LA = luminal area. N = number of mice. n = number of independent cardiomyocytes; PC = paricalcitol.

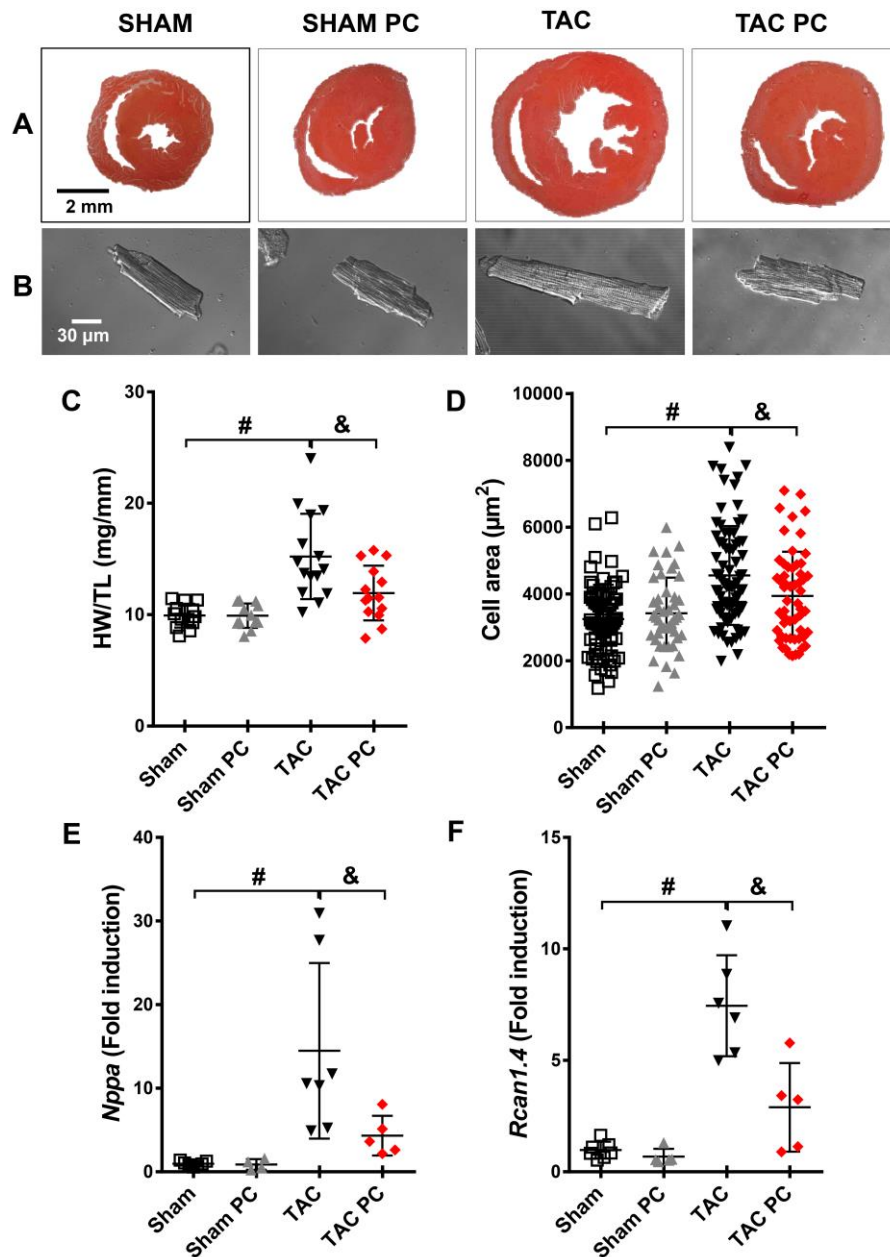


Figure 6. Paricalcitol treatment blunts hypertrophic development by attenuating the calcineurin/Rcan1.4 pathway (A) Representative examples of histological images of whole-hearts in axial views from sham, sham PC, TAC and TAC PC mice (B) Representative confocal microscopy images of adult cardiomyocytes. (C) TAC PC treated group has a ratio of HW (mg) to TL (mm) lower than that of the TAC group. Groups are sham (N=13), sham PC (N=12), TAC (N=15) and TAC PC (N=15). (D) Paricalcitol prevents cardiomyocyte hypertrophy. Groups are sham (n=72, N=6), sham PC (n=45, N=5), TAC (n=78, N=6) and TAC PC (n=56, N=6). (E, F) Real-time PCR analysis of mRNA expression of *Nppa* and *Rcan1.4*. Groups are sham (N=7), sham PC (N=5), TAC (N=7) and TAC PC (N=6). Data expressed as mean±SD. #p<0.05 sham vs. TAC. &p<0.05 TAC vs. TAC PC. HW = heart weight. TL = tibia length. N = number of mice. n = number of independent cardiomyocytes. PC = paricalcitol.

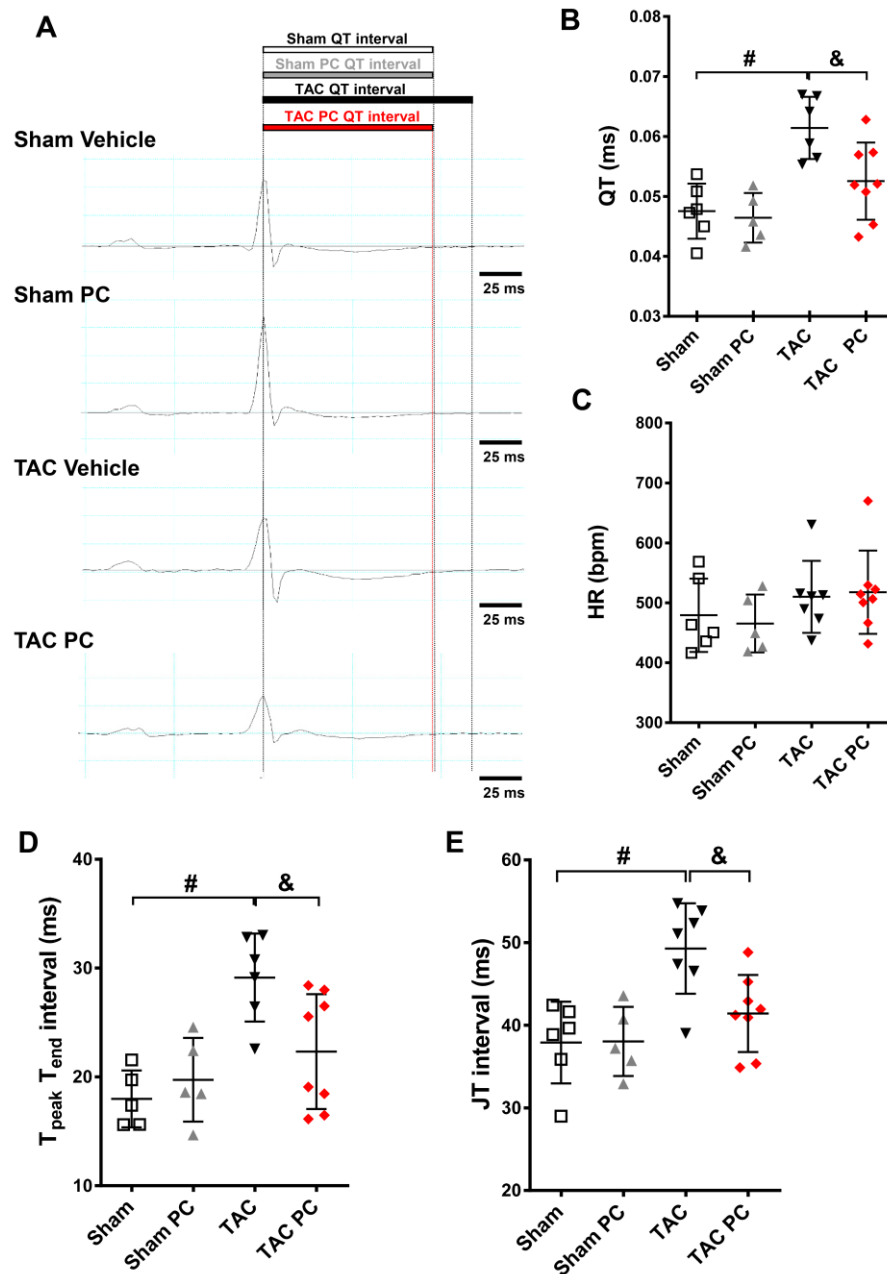


Figure 7. Long QT, JT and TpTe intervals associated with TAC 9 weeks after the surgery are prevented by paricalcitol treatment. (A) Representative examples of baseline ECG and QT interval measurement, (B) QT intervals, (C) HR, (D) JT interval and (E) TpTe interval values obtained in sham, sham PC, TAC and TAC PC groups 9 weeks after the surgery. Sham (N=6), sham PC (N=5), TAC (N=7) and TAC PC (N=8). Data expressed as mean \pm SD. #p<0.05 sham vs. TAC. &p<0.05 TAC vs. TAC PC. HR = heart rate; PC = paricalcitol.

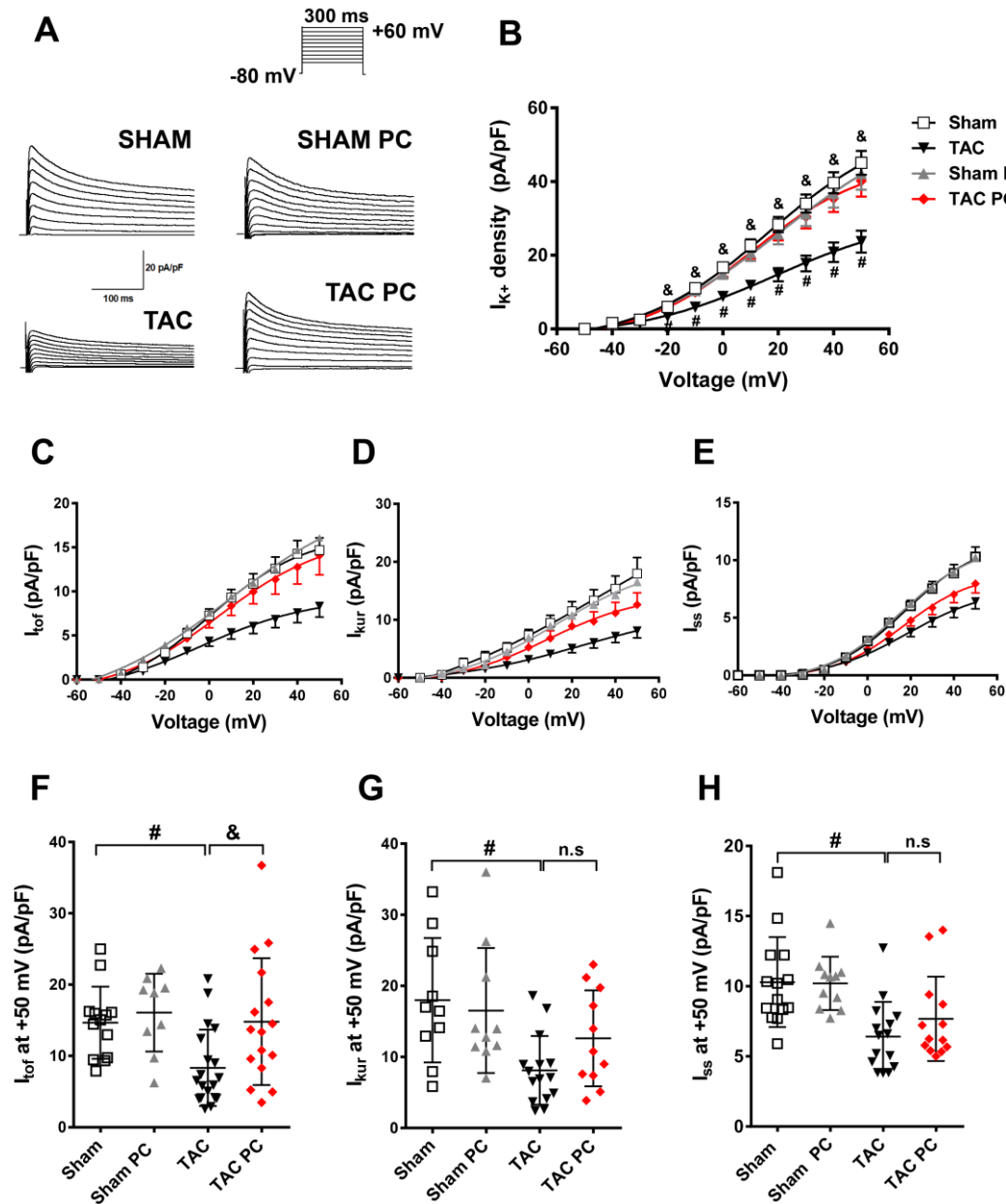


Figure 8. Paricalcitol treatment blocks the reduction of I_{K+} density and I_{tof} in myocytes isolated from mice 9 weeks after TAC surgery. (A). Representatives records of I_{K+} density obtained in 4 different myocytes isolated from sham, sham PC, TAC and TAC PC mice. The upper panel shows the protocol used to elicit I_{K+} . (B-E). Current density-voltage curves for I_{K+} (B) I_{tof} , (C) I_{kur} (D) and I_{ss} (E), obtained on myocytes isolated from sham, sham PC, TAC and TAC PC. Panel (F-G) shows individual values of I_{tof} , I_{kur} and I_{ss} densities recorded at +50 mV. Data expressed as mean \pm SEM for I/V curves and mean \pm SD for data at +50 mV. Sham (n= 13 for I_{K+} , n=13 for I_{tof} , n=10 for I_{kur} and n=14 for I_{ss}), sham PC (n= 10 for I_{K+} , n=9 for I_{tof} , n=10 for I_{kur} and n=11 for I_{ss}), TAC (n= 12 for I_{K+} , n=19 for I_{tof} , n=15 for I_{kur} and n=15 for I_{ss}) and TAC PC (n= 15 for I_{K+} , n=16 for I_{tof} , n=11 for I_{kur} and n=13 for I_{ss}) #p<0.05 sham vs TAC. &p<0.05 TAC vs TAC PC. n.s. = non-significant. n = number of independent cardiomyocytes. PC = paricalcitol